Polymer-assisted assembly of giant vesicles in physiological solutions

Alexis Cooper[a], Vignesha Vijayananda[b], Joseph Pazzi[b], Anand Bala Subramaniam[b*]

[a] Department of Chemistry and Biochemistry, University of California, Merced, Merced, CA 95343, United States.

[b] Department of Bioengineering, University of California, Merced, Merced, CA 95343, United States.

*Email: asubramaniam@ucmerced.edu

Abstract

Obtaining high yields of giant unilamellar vesicles (GUVs) in solutions of physiological ionic strengths is one of the major challenges in the use of GUVs in cell-mimicking applications. This is because the free energy cost for forming GUVs increases in solutions of high ionic strengths due increased adhesion between membranes. Gel coated glass slides used in gel-assisted assembly shows promise in assembling GUVs in salty solutions. However, only limited types of gel forming polymers are known to be effective. Extensive localized micrometer-scale dewetting of the polymer film from the substrate upon hydration results in low yields of GUVs from commonly used polymers such as agarose and polyvinyl alcohol. Furthermore, for polymers that show limited dewetting, increased temperatures, required for assembling GUVs composed of lipids with high transition temperatures, results in significant dewetting which limits the temperature at which assembly can occur. Here, we show that nanocellulose paper provides a facile means of suppressing dewetting of water-soluble polymers in the gel-assisted hydration method. With dewetting is suppressed, only low amounts of polymers are necessary to obtain high yields of GUVs. We show the significant extension of the temperature range of GUV assembly using paper supported gel-assisted hydration by assembling GUVs at high yield with raft forming mixtures that require assembly at 45 ºC. Moreover, we demonstrate that using nanocellulose paper as a substrate allows the assembly of GUVs from novel polymer classes such as biocompatible hyaluronic acid and dextran. We show the usage of scaled-down nanocellulose paper for the encapsulation of complex reactions in GUVs and the large scale assembly of GUVs for prototissue applications. Using nanocellulose paper as a substrate for polymer-assisted assembly of giant vesicles opens new avenues for using GUVs for biomedical and biophysical applications.

1. Introduction

Self-assembly of lipid films in low salt aqueous solutions into surface-attached micrometer-sized buds or volume-spanning "foam"-like mesophases is a precursor to the formation of cell-sized giant unilamellar vesicles (GUVs) via thin film hydration methods.[1,2] The GUV molar yield, *Y,* which is the amount of lipids in the membranes of the harvested GUVs relative to the amount of lipids deposited on the surface, reported as a percentage, was recently proposed to allow comparison between different conditions of assembly. The molar yield of GUVs is akin to the yield used in chemical synthesis, the reactant is the amount of lipid on the surface, and the product is the amount of lipid that ends up in the membranes of the GUVs. Qualitative categories classify the quantitative numbers into relative ranges, "negligible", $Y < 1$ % "low", $1 \leq Y < 10$%, "moderate", $10 \leq Y < 20$ %, "high", $20 \leq Y < 45$ % and "ultrahigh", $Y \geq 45$ %.

GUV yields obtained using thin film hydration methods, such as gentle hydration on glass slides, PAPYRUS, and electroformation were moderate or higher when performed using low salt solutions.[3] However, in salty solutions including those of physiological ionic strengths, the increased adhesion between the lamellar bilayers prevents the formation of buds on the surface or the formation of foam-like mesophases resulting in negligible yields of GUVs.[2] While GUVs encapsulating low salt solutions have myriad uses in biophysical and biological applications,[4–9] reconstitution of cellular proteins often requires a salty interior[10–17] marking a significant limitation to thin film hydration techniques. Depositing a dry thin film of partially soluble polymers such as agarose of various gelling temperatures or polyvinyl alcohol (PVA) onto glass slides prior to depositing the lipid allows the formation of GUVs in salty solutions.[18–20] The polymer films partially dissolve and exert an osmotic pressure against the stacks of membranes which overcomes the increased adhesion between the lipid bilayers.[18,20] GUV yields mostly ranged from low to

moderate. The highest measured yield, ~ 17 %, was only achieved for low gelling temperature (LGT) agarose at 22 ºC.[20] Agaroses of all other melting temperatures and polyvinyl alcohol (PVA) had yields below 10 %. LGT agarose at temperatures other than 22 ºC had yields of < 5 %. Polymers such as medium and high melting temperature agarose and PVA had insufficient dissolution while polymers such as ULGT agarose at 22 ºC and LGT agarose and ULGT agarose at elevated temperatures experienced dewetting from the glass substrate. Insufficient dissolution and dewetting both result in few GUV buds resulting in low yields and GUVs of small diameters.[20]

Here, we seek to address these limitations. We hypothesize that suppression of polymer dewetting from the substrate will allow the use of soluble polymers to obtain GUV yields of > 15 % in salty solutions. We test this hypothesis by considering the physicochemical causes of dewetting. We then address the causes by judicious selection of a natural nanostructured material, nanocellulose paper, as a substrate, and by controlling the surface concentration of the polymer. We find that with dewetting suppressed, a wide variety of soluble macromolecules, including biocompatible and biomedically relevant polymers such as hyaluronic acid and dextran, can be used to obtain GUV yields of > 15 % in salty solutions at a variety of temperatures. We demonstrate that this method effectively prepares GUVs encapsulating complex biochemical mixtures, including a commercial cell-free protein expression system capable of achieving ~100% deGFP expression, and monomeric G-actin and the bundling protein fascin that evolves to form bundled F-actin structures such as cortical rings and networks. The approach is highly adaptable, generating GUVs from paper pieces as small as 3 mm in diameter with 12 μL of buffer to sheets as large as 279.4 mm × 177.8 mm in 200 mL of buffer. Under the latter conditions, the method produces approximately 6×10^9 GUVs encapsulating physiological saline.

2. Results and Discussion

We first consider the evolution of a surface-attached film composed of partially soluble polymers in the context of assembling GUVs. The polymer film on the surface is prepared by spreading an aqueous polymer solution. Drying the aqueous polymer solution results in the formation of an amorphous glassy polymer film on the substrate. Lipids are then deposited onto the polymer film. Upon hydration, the lipids self-assemble to form stacks of lamellar lipid bilayers and water diffuses into the amorphous polymer layer forming a gel-like swollen layer. The swelling causes an increase in mechanical stress in the polymer layer. The stress can be relieved when the polymer molecules dissolve by disentangling and diffusing into the solvent,[21] which is the desired outcome for exerting osmotic pressure against the lamellar bilayers to form GUV buds. However, when the film adhesion to the substrate is poor, the stress can be relieved by dewetting the polymer film and the attached lamellar bilayers to form hybrid polymer-lipid pseudobuds instead of GUV buds.[20]

We reasoned that three material factors could reduce dewetting while preserving the ability of the polymer to dissolve and exert osmotic pressure on the lamellar bilayers: 1) A nanostructured surface could help prevent dewetting by providing pinning sites and breaking the polymer film into islands to provide gaps which could relieve swelling stresses prior to dissolution. 2) Surfaces with similar surface chemistry to the polymers could promote the wetting and adhesion of the solvent swollen polymer layer. 3) Low concentration of polymers to form thin films of polymers could reduce any transient mechanical stress anisotropy.

To test these three material factors, we choose nanocellulose paper as our model rough nanostructured substrate (Figure 1a, inset).[3] Unlike glass which is smooth (Figure 1b, inset), nanocellulose paper is composed of polydisperse entangled cylindrical fibers ~ 17 nm in radius and ~ 2 μm in length.[3] Cellulose is an insoluble polysaccharide with many terminal hydroxyl groups[22] and shares similar surface chemistry to water-soluble polymers. Cellulose, although

insoluble in water, swells in water, thus potentially matching the rate of swelling of the polymer and reducing the mechanical anisotropy between the polymer and substrate interface. Furthermore, although paper composed wholly of nanocellulose can be made from nanocellulose pulp, a substrate with a surface layer of densely-packed nanocellulose fibers can be obtained commercially at very low cost in the form of acid-free artist grade tracing paper.[3] For the purposes of assembling GUVs, these two substrates are indistinguishable.[3] We thus refer to tracing paper as nanocellulose paper.

To test simultaneously the effect of the surface concentration of the polymer and the identity of substrate on the assembly of GUVs, we use the polymer ultralow gelling temperature (ULGT) agarose. ULGT agarose dewets from glass coverslips when used to assist the assembly of GUVs resulting in yields of < 2 %.[20] We prepared surfaces with polymer nominal surface concentration, (polymer-NSC) of 0, 0.05, 0.5, 1.5, and 5.2 nmol/cm^2 , deposit 10 μg of 1,2-dioleoyl-*sn*-glycero-3-phosphocholine DOPC doped with 3 mol % of 1,2-dioleoyl-*sn*-glycero-3-phosphoethanolamine-*N*-[methoxy(polyethylene glycol)-2000] (ammonium salt) (PEG2000-DSPE) and 0.5 mol % TopFluor Cholesterol (TFC) and allow assembly to proceed for 1 hour in phosphate buffered saline (PBS). We report in Supporting Text and Table S1 the relative range of polymer-NSCs in the literature. Addition of 3 mol % of PEG2000-DSPE to the lipid mixture provides steric repulsion between the membranes to prevent aggregation of the GUV buds and GUVs in salty solutions (Figure S1). TFC allowed visualization of the membranes with confocal microscopy.

To obtain GUVs, we use a pipette to apply fluid shear to harvest any buds that formed on the substrates. We then quantified the distribution of sizes, counts, and calculated the molar yield of the GUVs (Figure 1a,b) via previously established image analysis procedures.[3,20] We show

representative images of the harvested objects and histograms of the size distributions of the GUVs from the glass and nanocellulose paper surfaces in Figure S2 and S3 respectively. We find that the yield of GUVs evolved non-monotonically with the polymer-NSC for both glass and nanocellulose paper. This result shows the multivariate effect of substrate identity and the polymer-NSC on the assembly of GUVs. Absent any ULGT agarose, the molar yield was negligible, < 1 %, for both surfaces. Furthermore, there were hardly any lipid structures, i.e. GUVs, multilamellar vesicles (MLVs) or lipid debris, in the solution, indicating that most of the lipids remained on the surfaces (Figure S2). For both surfaces, the yield increased before reaching a peak and then decreased with an increase in the polymer-NSC. The peak yield from the ULGT agarose-coated glass slide was 10 ± 1 % and was obtained at a polymer-NSC of 0.5 nmol/cm^2. The peak yield from the ULGT agarose-coated nanocellulose paper was double that of the ULGT agarose-coated glass slide at 21 ± 1 % and was obtained at a polymer-NSC of 1.5 nmol/cm^2. A polymer-NSC of 5.2 nmol/cm^2 resulted in a decrease in the molar yield to 2 ± 1 and 13 ± 1 % for ULGT agarose-coated glass slides and ULGT agarose-coated nanocellulose paper respectively. For all the polymer-NSCs tested, ULGT agarose-coated glass slide had a higher molar yield than ULGT agarose-coated glass slides. These differences in yield have practical consequences. Figure 1c, d show that the number of large GUVs with diameters > 10 μm was strongly linearly correlated with the molar yield of GUVs (Figure 1c, Pearson's R=0.9933; Figure 1d, Pearson's R=0.9607). This result demonstrates that obtaining GUVs desired for most biophysical experiments, that is, GUVs > 10 μm, use of surfaces that produce the higher molar yield is advantageous. Additionally, a fortuitous observation was that the samples harvested from the ULGT agarose-coated nanocellulose paper consistently had lower amount of lipid debris, aggregates, and other non-GUV structures in the solution compared to the samples harvested from the ULGT agarose-coated glass surface. This observation

held even when the molar yield of GUVs was similar on the two surfaces with different polymer-NSCs (Figure 1e, f white arrows).

To understand the peaked evolution of the GUV yields and the lower amount of lipid debris from ULGT agarose coated-nanocellulose paper, we obtained images of the lipid film on the surface prior to harvesting. We find that the surfaces were covered with varying fractions of lamellar bilayer stacks, GUV buds, and hybrid lipid-polymer "pseudobuds" (Figure 2). Lamellar bilayer stacks appeared as flat fluorescent regions (yellow arrows), GUV buds appear spherical with uniform intensity (white arrows), and hybrid lipid-polymer pseudobuds have micrometer-sized dark non-fluorescent region at their base (red arrows). No foam-like mesophase was apparent. When harvested, the GUV buds self-close to form GUVs and the lipid-polymer pseudobuds form MLVs and other lipid debris. There were large areas of lipid bilayer stacks on both surfaces at the lowest polymer-NSC of 0.05 nmol/cm^2 (Figure 2a, b, yellow arrows). We interpret that these regions did not have sufficient polymer dissolution to overcome the increased adhesion of the bilayers in PBS. At the polymer-NSC corresponding to their respective peak yields, the surfaces had a high fraction of GUV buds. Polymer-coated nanocellulose paper had a large number of GUV buds and a lower fraction of pseudobuds compared to the glass surface (Figure 2c,d). Above the polymer-NSC corresponding to the peak yield, both surfaces had large numbers of pseudobuds and large dark areas (Figure 2e, f). The dark areas are indicative of dewetting and lift-off of the lipid and polymer. We conclude that both the surface topography of nanocellulose paper and lower polymer-NSCs effectively suppresses polymer dewetting and reduces the formation of lipid-polymer pseudobuds. The suppression of dewetting increases GUVs yields in salty solutions. Additionally, the reduced formation of pseudobuds on the nanocellulose paper surface explains the reduced amount of lipid debris relative to the glass surface.

Having shown that nanocellulose paper suppresses polymer dewetting, increases yields, and decreases lipid debris, we next sought to test the limits of the polymer-coated nanocellulose paper for functional assembly of GUVs at different temperatures. Previously, we had found that assembly at temperatures of ≥ 37 ºC resulted in a greatly reduced yield of GUVs using LGT and ULGT agarose-coated glass coverslips. We attribute this observation to temperature-induced polymer dewetting of the polymer films. To test the utility of polymer-coated nanocellulose paper for assembling GUVs at elevated temperatures, we use a canonical phase separating raft mixture consisting of DOPC:1,2-dipalmitoyl-*sn*-glycero-3-phosphocholine (DPPC):Cholesterol:DSPE-PEG2000:1,2-dioleoyl-*sn*-glycero-3-phosphoethanolamine-*N*-(lissamine rhodamine B sulfonyl) (ammonium salt) (Rhod-PE):TFC at a mol % of 36:33:27.5:3:0.25:0.25 as our model lipid mixture. The chain melting temperature of DPPC is 41.5 ºC [23] and thus we assembled the GUVs at 45 ºC. In addition to higher than room temperature assembly, GUVs are often assembled at low temperatures, 4 ºC, to prevent premature reaction when constructing synthetic cells[10–12,24] . Additionally for future cold-chain biomedical applications, assembly and storage of GUVs at low temperature could be useful for reducing the activity of degradative enzymes, the rate of intrinsic biomolecule degradation, and the rate of growth of microorganisms. To test for assembly at low temperatures, we assemble GUVs using DOPC at 4 ºC. The chain melting transition temperature of DOPC is – 17 ºC.[25]

The yield of phase separating GUVs was 17 ± 3% and the yield of the DOPC GUVs was 22 ± 2 % on the ULGT-coated nanocellulose paper (Figure 3a). The phase separated GUVs appear to have equal composition of L_d and L_o phases (Figure 3b). This result is consistent with recent reports that methods using the hydration of thin lipid films largely have the composition of the lipid stock.[26] We show a representative image of the DOPC GUVs assembled at 4 ºC and

histograms of the size distributions in Figure S4 and S5. We conclude that with dewetting suppressed, the polymer-coated paper can be used to efficiently assemble GUVs of different compositions at a variety of temperatures in salty solutions.

Assembly of GUVs via the polymer-assisted technique necessarily leads to incorporation of polymers in the GUVs.[20] Since incorporation of polymers is a necessary feature of the technique, we explored if there are limits on the identity of the polymer. Thus far, extant reports use gel-forming or cross-linked polymers on smooth glass surfaces, overwhelmingly ultra-low gelling agarose and PVA.[18,19,27,28] We choose from a selection of highly soluble polymers to provide the greatest contrast with extant reports that use cross-linked polymers or gel-forming polymers.[18,19,27–34] We use three different polysaccharides, hyaluronic acid, dextran, carrageenan, and a polypeptide, poly-D-lysine. These polymers are used in biomedical applications[30–36] due to their biocompatibility or different modes of degradation in the body [37–39]. Hyaluronic acid (HA) is an anionic polymer used to promote wound healing, in tissue engineering, and in cosmetics.[32] Dextran is an FDA-approved plasma expander,[40] a contrast agent for magnetic resonance imaging[41], and, when chemically cross-linked, is used for tissue engineering.[42,43] Carrageenan is a gel-forming polymer used as scaffolds in tissue engineering,[36] in drug delivery applications,[33,34] and as a common food additive[33]. Polylysine is used extensively as a promoter for cell adhesion in cell-culture.[44] We used HA of two different molecular weights, 8-15 kDa and 70-120 kDa, and dextran of two different molecular weights, 6 kDa and 100 kDa. We also tested salmon DNA and bovine serum albumin (BSA), which are not used for biomedical applications but have different macromolecular and chemical characteristics. Salmon DNA is a nucleic acid and BSA is a globular protein. We screened various surface concentrations and assembly conditions (See Methods) and report the highest GUV yield and the corresponding polymer-NSC in Table 1.

We find that most of these molecules when coated on nanocellulose paper support the formation of GUVs at moderate to high yields, 13 - 22 %, at the various temperatures of assembly that we tested. HA 8-15 kDa results in a high yield of 20 ± 0.8 %, 22 ± 2.5 %, and 18 ± 2.2 % at 4 ºC, 22 ºC and 45 ºC respectively. Dextran had a yield of 18 ± 0.7 % and 15 ± 0.3 % at 4 ºC and 22 ºC. Poly-D-lysine had a high yield of 19 ± 3.0 % at 22 ºC. Use of nanocellulose paper as a substrate was essential for obtaining high yields of GUVs using these highly soluble polymers. Use of glass as a substrate resulted in massive dewetting of the lipid and polymer films and negligible yield of GUVs (Figure S6). DNA and BSA assisted in the assembly of GUVs compared to the bare nanocellulose paper surface, but the yields of GUVs were low, 7 ± 1 % and 6 ± 1 % respectively.

We find no apparent correlation between the molecular weight and polymer-NSC with the yields (Table 1). This observation is consistent with more than one process, interactions with the membrane, dewetting, and solubility affecting the assembly.[20] Thus, polymer-NSC must be optimized for each novel macromolecule. We show additional results from our screen of various polymers, polymer-NSC, and temperatures in Tables S2 and S3. We surmise that a range of macromolecules can be used to assist the assembly of GUVs in salty solutions when dewetting is suppressed.

Since obtaining GUVs in salty solutions is desired to reconstitute biochemical reactions within cell-like confines and to assemble synthetic cells, we tested the polymer-coated nanocellulose paper's ability to reconstitute two "difficult" reactions, cell-free transcription translation (TXTL) expression of proteins from a nucleic acid template[24] and the reconstitution of actin bundles. Cell-free expression mixtures that are commercially available are proprietary mixtures of proteins and salts. Reconstitution of actin bundles requires the encapsulation of G-

actin and bundling proteins in monomeric form prior to actin polymerization and bundling in GUVs.[10,11,14,45]

We encapsulate a cell-free protein expression mixture (myTXTL® Pro) with 5 nM (13.4 ng/μL) of T7 deGFP plasmid. Successful expression results in the formation of green fluorescent protein (GFP) which can be imaged with fluorescence microscopy. To perform the reaction, we cut the polymer-coated paper into a 3 mm diameter disk to scale down our typical assembly volume by 12.5× to the 12 μL volume recommended by the manufacturer. We perform the assembly in a 0.5 mL PCR tube for convenient fluid management (Figure 4a). The GUV buds were allowed to assemble at 4 ºC to reduce premature expression of deGFP. After 1 hr we harvested the GUV buds to obtain GUVs and then incubated the suspension at room temperature for 6 hours to allow gene expression. We then imaged the GUVs using dual-channel confocal microscopy. Figure 4b shows representative images of the harvested GUVs. The method resulted in ~ 1.41×10^5 GUVs in the chamber. We show in Figure 4c, a histogram of the luminal intensity of n = 660 GUVs. The mean intensity of the lumen was 25 ± 8 arbitrary units (AU), and the lowest measured intensity was 5.5 AU. The coefficient of variation (CV) was 0.30. The results of a second independent repeat are shown in Figure S7. In contrast, the mean intensity of a control that was prepared and imaged identically but with plasmid omitted was 3 ± 1 AU with the highest measured intensity of 5 AU. We conclude that 100% of the GUVs prepared with the T7 deGFP plasmid had measurable gene expression for the first sample, and 98% of GUVs for the second sample. Previous reports encapsulating commercial PURE systems using the emulsion transfer technique with 10 ng/μL of template DNA resulted in 87 % of the GUVs having measurable GFP expression[24] and a bead-based freeze thaw technique with 7.4 nM template DNA reported 30% of the GUVs having measurable YFP expression[12]. Reported CVs of GFP intensity for the inverted emulsion technique

is between 0.3 and 0.5.[15,16] The CV for YFP intensity expressed in the lumens of the GUVs from the bead-based freeze thaw technique was not reported.

To obtain actin bundles in GUVs, we encapsulate 12 μM actin with 1.8 μM fascin using a 12 μL reaction volume at 4 °C. Similar to the cell-free expression experiments, we performed the reaction at 4 ºC to reduce the premature polymerization of G-actin into F-actin during the encapsulation process. Figure 5d-e shows the maximum intensity projections of a confocal Z-stacks of the GUVs. We limited our analysis to GUVs that had diameters ≥ 6.5 μm since it was difficult to discern actin bundles in small GUVs. We find that 74% of GUVs had actin bundling using an upright confocal laser-scanning microscope equipped with a 20× NA 1.0 Plan Apochromat objective (Figure S8). Due to the low image resolution and movement of GUVs, it was difficult to discern the morphology of the actin bundles present in the GUVs. To overcome this, we prepare a second independent sample, bind the GUVs to the surface of a coverslip, and obtain superresolution images of the actin bundles in the GUVs (Figure 5d-e). We find that 87% of the GUVs had actin bundling inside the lumen (N=53, Figure 5f). Of the GUVs with actin bundling, 26 % of GUVs have actin rings, 54 % have ring-like structures, and 20 % have networks of actin bundles (N=46). We estimate that there were 1.5×10^4 GUVs in the chamber. Furthermore, as expected, increasing the actin concentrations to > 24 μM resulted in GUVs with multiple bundles and protrusions (Figure S9). We conclude that the polymer-coated nanocellulose paper allows for high yield of GUVs that can efficiently encapsulate complex biochemical mixtures.

In addition to scaling down, the technique can also be scaled up to obtain large numbers of GUVs by spreading the polymer solution onto large pieces of paper. We show an example of a protocol that can be performed in a typical laboratory using a commercial baking tray and a piece of paper 27.9 cm × 17.8 cm (11-in × 7-in). We use dextran-coated paper since dextran has a lower

cost compared to the other polymers (Supporting Table S4). We obtain 188 mL of suspension (Figure 5a) containing a total of 5.5×10^9 GUVs in a single preparation that takes approximately 2.5 hours. We show the histogram of sizes in Supporting Figure S10. Figure 5b shows a representative image of a tissue-like assembly with a size of 5900 μm × 5900 μm × 35 μm by concentrating the GUVs via centrifugation. Figure 5c shows that the number of GUVs obtained from the scale up is 28× more than what is obtained from all wells in a 48-well plate. Furthermore, a large piece of paper stored on a room temperature laboratory bench can be used for up to 21 days without significant loss of GUV yield or apparent reduction in the quality of GUVs with storage time (Figure 5d-e). After 28 days of storage, although the yield falls significantly, the GUVs that were harvested appeared identical to those obtained at earlier times. Storing the paper at 4 °C, prevented this apparent slow degradation of the properties of the polymer-coated paper, and there was no reduction in yield when the paper was retrieved from the refrigerator after 28 days. However, repeated removal of the tracing paper from the refrigerator should be avoided since it results in condensation which decreases the yield with each removal (Figure S11).

3. Conclusion

In conclusion, we show that by using nanocellulose paper as a substrate, the range of polymers that can be used to assist the assembly of GUVs in salty solutions is increased significantly to include at least 6 soluble macromolecules, hyaluronic acid, dextran, carrageenan, poly-D-lysine, BSA and DNA. We find that by using nanocellulose paper as a substrate, we can prevent dewetting resulting in high yields of GUV from a wide range of assisting macromolecules, and that we can assemble high yields of GUVs in salty solutions from 4 °C to at least 45 °C. Additionally, polymer-coated nanocellulose paper allows for convenient experimentation. A large piece of paper can be prepared in a few hours and then used to assemble large quantities of GUVs in hundreds of mL of

liquid or cut to sizes that fit into disposable plasticware such as well plates and Eppendorf tubes to assemble GUVs in tens to hundreds of μL of liquid. The paper can also be prepared in advance and stored for use later. Thus, we anticipate that the polymer-coated nanocellulose paper that we report here and possibly other polymers that we did not test will be useful for assembling GUVs in salty solutions for various biophysical and biomedical applications.

4. Experimental Section

Materials

We purchased premium plain glass microscope slides (75 mm × 25 mm), 48-well polystyrene tissue culture plates (Fisherbrand), Fisherbrand™ Ultra-Clean™ Supreme Aluminum Foil, glass coverslips (Corning, 22 mm × 22 mm), Falcon™ Bacteriological Petri Dishes with Lid, 2 mL disposable glass Pasteur pipettes, dropper bulb, 4 mL glass vials, 50 mL Falcon centrifuge tubes, Grafix art Shrink film (8.5-in × 11-in), and Eisco™ Mixed Set of Glass Delivery Tubes from Thermo Fisher Scientific (Waltham, MA). We purchased acid-free artist grade tracing paper from Jack Richeson and Co. Inc, and Ziploc slider bags (10.5-in × 9.5-in × 2.6-in) on Amazon. (Seattle, WA, USA).

Chemicals

We purchased sucrose (BioXtra grade, purity ≥ 99.5%), glucose (BioXtra grade, purity ≥ 99.5%), casein from bovine milk (BioReagent grade), agarose type IX-A: ultra-low gelling temperature (Catalog number: A2576, molecular biology grade), agarose: low gelling point (Catalog number: A9414, molecular biology grade), deoxyribonucleic acid, single stranded from salmon testes (D7656), carrageenan (C1013), dextran from *Leuconostoc spp*. (Catalog number: 09184, MW: 100,000), bovine serum albumin (Catalog number: A3059), hyaluronic acid sodium salt from *Streptococcus equi* (Catalog number: 40583, MW: 8,000 – 15,000) and (Catalog number: 96144 MW: 70,000 – 120,000), poly(vinyl alcohol) (Catalog number: 363138, MW: 31,000-50,000, 96-99% hydrolyzed) and (Catalog number: 363065, MW: 146,000-186,000 99+% hydrolyzed) from Sigma-Aldrich (St. Louis, MO). We purchased dextran from *Leuconostoc mesenteroides* (Catalog number: J62775, MW: 6,000) from Alfa Aesar (Ward Hill, MA). We purchased chloroform (ACS grade, purity ≥ 99.8%, with 0.75% ethanol as preservative), 96% ethanol (molecular biology

grade) and Invitrogen 10× phosphate buffered saline (PBS) (pH 7.4, 0.2 µm filtered, 1.37 M sodium chloride, 0.027 M potassium chloride, 0.080 sodium phosphate dibasic, 0.020 M potassium phosphate monobasic) from Thermo Fisher Scientific (Waltham, MA). We obtained 18.2 MΩ ultrapure water from a Milli-Q® IQ 7000 Ultrapure Lab Water System (Burlington, MA). We purchased 1,2- dioleoyl-*sn*-glycero-3-phosphocholine (18:1 (Δ9-cis) PC (DOPC)), 23-(dipyrrometheneboron difluoride)-24-norcholesterol (TopFluor-Chol), cholesterol (ovine wool, >98%), 1,2-dipalmitoyl-*sn*-glycero-3-phosphocholine (16:0 PC (DPPC)), 1,2-dioleoyl-*sn*-glycero-3-phosphoethanolamine-N-(lissamine rhodamine B sulfonyl) (ammonium salt) (18:1 Liss Rhod PE) and 1,2-distearoyl-*sn*-glycero-3-phosphoethanolamine-N-[methoxy(polyethylene glycol)-2000](ammonium salt) (PEG2000-DSPE) from Avanti Polar Lipids, Inc. (Alabaster, AL).

Procedure for cleaning paper

A single piece of tracing paper was cut into 1/8th sections and placed in 250 mL of 96 % molecular biology grade ethanol in a glass crystallizing dish (45 mL, dish diameter × height 40 mm × 25 mm) for 15 minutes. The liquid in the dish was manually agitated occasionally. After 15 minutes the ethanol was discarded and the process repeated once. 250 mL of Type I ultrapure water was then added to the dish, swirled three times and discarded. This process was repeated an additional three times. Then 250 mL of Type I ultrapure water was added to the dish and allowed to soak for a further 15 minutes with occasional manual agitation. The water is then discarded and the process repeated once. Then the individual papers are removed and placed on aluminum foil and another piece of foil was placed on top loosely to not contact the paper surface before placing the paper sheets in a 65 ºC oven overnight. The next day we remove the paper and store it in a 150 mm diameter polystyrene Petri dish on a lab bench until further use.

Fabrication of polymer-coated tracing paper and glass slides

For general fabrication of paper, we coat the whole strip of cleaned paper (3-in × 4.5-in) by placing the paper on 4-inch wide Parafilm on a hotplate set at 40 ºC. 5.4 mL of 0.3 w/w % ULGT agarose is applied in a sinusoid snake-like manner across the length of the paper. Then a clean L-shaped glass delivery tube (18 cm × 6 cm) was passed over four times back and forth along the length of the paper, careful to ensure no agarose spills over the sides of the paper. The paper is allowed to dry on the hotplate for 4 hours. Once dried, the paper is stored in a 150 mm polystyrene Petri dish with the agarose-coated side facing up and not in contact with any surfaces. Each paper sheet can be used to prepare approximately 50 9.6 mm disks for use in the 48-well plate.

For comparison of GUV assembly characteristics between polymer-coated glass slides and polymer-coated paper, we spread the polymer solution identically. Since the glass coverslips were 22 mm × 22 mm squares, we cut the nanocellulose paper to 22 mm × 22 mm squares. We then place the paper on a piece of Parafilm on a hotplate set at 40 °C. We apply 300 µL of solutions consisting of the polymers of various weight percents on the substrates. The polymer solution was evenly spread on the substrates with the side of a 1000 µL pipette tip. The substrates were left on the hotplate for 4 hours to ensure the substrates were completely dry. Polymer-coated tracing paper and coverslips were stored face up in a clean Petri dish and used within 24 hours.

For polymer coated glass slides, we use 25 mm × 75 mm glass slides placed on a piece of Parafilm on a hotplate set at 40 °C and apply 1,162 µL of polymer solution. We spread the solution evenly with the side of a 1000 µL pipette tip. The glass slides were left on the hotplate for 4 hours to ensure the slides were completely dry. The slides were stored face up in a clean Petri dish and used within 24 hours.

Deposition of lipids

We deposit lipids as described previously.[1,20] Briefly, we cut circular disks of the polymer coated tracing paper using a circle hole punch (EK Tools Circle Punch, 3/8 in.). We deposited 10 μL of the lipid solution onto the polymer-coated side of the tracing paper evenly using a glass syringe (Hamilton) while holding the paper with metal forceps. The coated nanocellulose paper disks were placed on a clean glass slide and into a standard laboratory vacuum desiccator for 1 hour to remove traces of organic solvent prior to hydration.

Procedure for assembly

We hydrate as previously described to ensure standardized conditions that allow for comparison between samples.[1,20] The coated nanocellulose paper disks were placed into individual wells in a 48-well plate for hydration. We add hydration buffer to the wells with coated nanocellulose paper disks with a pipette and cover the samples with the lid of the well plate to minimize evaporation. The volume and hydration buffer varied depending on the temperature of assembly. All hydration and sedimentation buffers are made as needed from stock solutions of 1 M sucrose, 1 M glucose, and 10 × PBS and used within 1 hour. 1 M sucrose and glucose stock solutions are stored in a 4 °C fridge and used for a maximum of two weeks. If solutions are used past this time, we find that the yield of the controls had a high likelihood of being low. Occasionally even when all protocols are followed the yield fell. In these cases, remaking the buffers and performing the controls restored yields.

For samples assembled at 4 °C, the buffers and the 48-well plate were prechilled to 4 °C in an Isotemp™ low temperature incubator (model number: 3724, Fisher Scientific, Waltham, MA) for at least 1 hour. The coated tracing paper was placed inside of the prechilled 48-well plate and cooled for a further 5 minutes. We add 150 μL of the prechilled hydration buffer to the well plate

and allow the samples to hydrate inside the low temperature incubator, for 1 hour. For experiments probing the effects of incubation time we varied the time to 2 hours and 24 hours.

For samples assembled at 22 °C, low salt samples were hydrated in 100 mM sucrose and high salt samples were hydrated in 100 mM sucrose in 1× PBS. We add 150 µL of the hydration buffer to the well plate and allow the samples to hydrate for 1 hour on a laboratory bench at room temperature. For experiments probing the effect of incubation time, we increased the time to 2 hours

For samples assembled at 37 °C, low salt samples were hydrated in 100 mM sucrose and high salt samples were hydrated in 100 mM sucrose in 1× PBS preheated to 37 °C using a dry heating block (Multi-Blok Heater, Thermo Scientific). We preheat the 48-well plate on a hotplate set at 37 °C for 1 hour. The coated tracing paper was placed inside of the preheated 48-well plate and allowed to preheat for 5 minutes. We add 150 µL of the preheated hydration buffer to the well plate and allow the samples to hydrate for 1 hour on the hotplate.

We assemble GUVs at 45 °C on glass as previously described.[2] For samples assembled at 45 °C on tracing paper, 160 µL of 94 mM sucrose or 94 mM sucrose in 0.94× PBS was used to account for the 10 µL loss from evaporation. The hydration solutions were preheated to 45 °C using a dry heating block. We preheat the 48-well plate on a hotplate set at 45 °C for 1 hour. The coated tracing paper was placed inside of the preheated 48-well plate and allowed to continue preheating for a further 5 minutes. The films were allowed to hydrate on a hotplate set to 45 °C.

Procedure for harvesting the GUVs

We harvest GUVs from the substrates as previously described at the temperature of assembly.[2] We detach the GUVs from the substrate by pipetting 100 µL of the hydrating solution with a cut 1000 µL pipet tip on 6 different regions of the coated tracing paper to cover the whole area. On the 7th

time, we aspirate all the GUV containing solution and transfer the liquid into a 0.5 mL Eppendorf tube. From tracing paper, the final sample volume was ~135 μL with ~15 μL that appears to be lost during the harvesting. From glass, the final sample volume was ~150 μL. We take a 20 μL aliquot of the GUV suspension and measure the osmolarity of the solution using a freezing point depression multi-sample osmometer (Model 2020, Advanced Instruments, USA).

Large scale-assembly of GUVs using a whole sheet of tracing paper

We adapt the procedure for large scale assembly with modifications.[3] We place a 279.4 mm × 177.8 mm (11-in. × 7-in). piece of nanocellulose paper on a clean sheet of aluminum foil. Then, 4.25 mL of a 2.16 w/v % solution of dextran with a molecular weight of 100 kDa was spread on the left side of the paper using a bent glass delivery tube with dimensions of 18 × 6 cm. The process was repeated for the right side of the paper to cover the paper. The final nominal surface concentration of dextran 100 kDa obtained on the paper was 4.34 nmol/cm^2. We then placed the paper in an oven set to 40 ºC and left it in the oven for 5 hours. We used a similar procedure to spread the lipid solution in chloroform in a chemical safety hood. The lipid solution consisted of DOPC:DSPE-PEG2000:TopFluor Cholesterol at 96.5:3:0.5 mol % dissolved in chloroform at a concentration of 3.5 mg/mL. The lipid-coated paper was placed into a standard laboratory vacuum chamber for 1 hour to remove trace amounts of organic solvent. We then place the lipid coated tracing paper in a 13-in. × 11-in. baking tray (inner dimension 11.4-in × 7.4-in) with PTFE magnetic stir bars placed on the corners of the paper to prevent curling of the paper upon hydration. The paper was hydrated with 200 mL of 1× PBS+ 100 mM sucrose. We incubate the sample for 1 hour before removing the stir bars. We harvest the GUVs using an acrylic shrink film of dimension 5-in × 7.4-in by moving it across the surface of the nanocellulose paper in one direction while applying gentle pressure to detach the GUV buds from the surface. The process is repeated. We

transfer the solution containing the GUVs into four 50 mL Falcon tubes for storage. Quantification was conducted immediately after GUV assembly. For quantification, we take 2 μL of the GUV solution and sediment in 58 μL of the 1×PBS+100 mM glucose for 3 hours before imaging. To obtain the prototissue image shown in Figure 5b, we mix 7.5 mL of the sample with 7.5 mL of 1×PBS+100 mM glucose in a 15 mL Falcon tube and centrifuge at 2080 × g for 30 minutes to pellet the GUVs. We remove 14 mL of the supernatant. We take a 10 μL aliquot from the bottom of the remaining 1 mL and mix it with 50 μL of 1× PBS+100 mM glucose and placed the suspension into the imaging chamber. We allowed the GUVs to sediment for 3 hours before imaging to obtain a close packed layer of GUVs. A close-packed layer of GUVs approximately 5900 μm × 5900 μm × 35 μm high (length × width × height) custom PDMS chamber.

Control procedure

To control batch-to-batch variations of the dry DOPC powder obtained from the manufacturer, we prepare GUVs using 1.0 mg/mL of DOPC:TopFluor Cholesterol 99.5:0.5 using the standardized PAPYRUS procedure[1,3] using freshly prepared buffers and paper. We measure the molar yield. If the yield was below 33 ± 2 % we infer that the mass of DOPC was different from the stated nominal mass. To correct this difference, we assemble GUVs by applying 0.8 mg/mL, 1.0 mg/mL, and 1.2 mg/mL of the nominal concentration. We calculate the molar yield assuming an applied lipid amount of 10 μg. We renumber the concentration of lipid that resulted in a yield of 32 ± 2 % as 1 mg/mL. We find that ~ 1 in 10 DOPC lipid vials from the manufacturer had an apparent lipid concentration that was different than what was reported.

To control experimentalist variations, we ensure that the experimentalist is able to obtain at least three independent measurements on three separate days that had MY of 33 ± 2 % and distribution of sizes similar published distributions following established procedures for lipid

deposition, hydration, and harvesting. Reproducing previously published results served as a check for the user's skill and care in performing assembly before trying new conditions of assembly with unknown yields. Lower than expected yields with validated lipid and buffer are often due to incorrect lipid deposition techniques (allowing the lipid to coat the underside of the paper for example) or inefficient harvesting.

Confocal microscopy

Imagining of the harvested and free-floating vesicles was conducted as previously described. We construct imaging chambers by placing poly(dimethylsiloxane) (PDMS) chambers with dimensions of 5.9 mm × 5.9 mm × 1 mm (length × width × height) on glass microscope slides. We passivate the chamber with 1 mg/mL casein in PBS before use to prevent the rupture of GUVs on the surface of bare glass. We thoroughly rinse the chambers with ultrapure water after passivation by gently pouring 50 mL of water from a 50 mL Falcon tube over the chambers three times. We sediment the GUVs in glucose in either ultrapure water or 1× PBS. We balance the osmotic pressure between the GUV suspension and the sedimentation solution by modifying the concentration of glucose. We fill the passivated chamber with 58 µL of the sedimentation solution. We pipette 2 µL aliquot of the harvested GUV suspension in the middle of the chamber, aspirate the solution and deposit in the middle of four quadrants and then the mid-section of the chamber to ensure even distribution of the GUVs. We cover the sedimentation chambers with a glass cover slip and allow the GUVs to sediment for 3 hours in a covered 150 mm Petri dish with moistened Kimwipe to minimize evaporation. We use an upright confocal laser-scanning microscope (LSM 880, Axio Imager.Z2m, Zeiss, Germany) with a 10× Plan-Apochromat objective with a numerical aperture of 0.45 to capture images. We image using an automated tile scan and focus routine (49 images [5951.35 µm × 5951.35 µm, (3212 pixels × 3212 pixels)]) to capture the entire area of the

chamber. For vesicles labeled with TopFluor cholesterol, we use a 488 nm argon laser. We set the pinhole to 15.16 Airy units which gave a confocal slice thickness of 79.3 μm. For phase separated vesicles we capture dual-channel images. We use a 488 nm argon laser and a 561 nm diode-pumped solid-state laser. We image using the line-switching scanning mode. We set the pinhole of the rhodamine channel to be 14.57 Airy units which gives a confocal slice thickness of 79.4 μm. We set the pinhole of the TopFluor cholesterol channel to be 17.76 Airy units which gives a confocal slice thickness of 79.4 μm. We normalize the laser power by measuring the intensity of 10 vesicles with diameters between 9 and 11 μm from 3 images using the line tool in FIJI. We compare the measured intensity to 10 vesicles with diameters between 9-11 μm from a previous tile scan to ensure that the average intensity remains consistent within a range of 59 ± 3 arbitrary intensity units. We adjust the laser power so that the intensity is within one standard deviation of the average.

For Figure 2 we obtain confocal Z-stacks of hydrated lipid coated surfaces at various concentrations of the polymer. We use an upright confocal laser-scanning microscope (LSM 880, Axio Imager.Z2m, Zeiss, Germany) with a 20× Plan-Apochromat objective with a numerical aperture of 1.0. We scan the whole surface and capture a Z-Stack (135 images [151.8 μm × 151.8 μm, 1272 pixels × 1272 pixels, slice interval 0.75 μm]) to image from the surface of the substrate to 99.87 μm above the surface on a region that is representative of the surface.

Determination of optimal polymer surface concentration

We use an upright confocal laser-scanning microscope (LSM 700 Axio Imager.Z2m, Zeiss, Germany) with a 10× Plan-Apochromat objective with a numerical aperture of 0.45 to examine and capture images. In general, surfaces that do not have buds will not have high yields and those surfaces are not considered. For surfaces that have apparent buds, the buds are examined for evidence of dewetting patterns to distinguish GUV buds from pseudobuds. Surfaces that show low

amount of pseudobuds and high number of GUV buds are chosen as optimal concentration. On some surfaces, distinguishing surfaces with a higher number of buds compared to pseudobuds was challenging. For these surfaces, the buds are harvested, and the molar yield is measured for both the concentrations. Only the concentration of the highest molar yield is reported in the main text. Any additional tilescans and yields are provided in Table S3-4 for completeness.

Characterization of long-term functionality of polymer-coated papers

Two separate pieces of ULGT agarose paper were stored at 4 °C and 22 °C in 150 mm polystyrene Petri dishes with the agarose coated side facing up and not in contact with any surfaces. We assemble GUVs from both stored pieces of agarose paper and measure the molar yields at 4, 7, 14, 21 and 28 days. We additionally assemble GUVs from a piece of agarose coated tracing paper stored at 4 °C for 28 days without removal from the low temperature storage.

myTXTL expression of eGFP

We deposit 10 µg of lipid on a 9.5 mm diameter disc of tracing paper. We place the lipid coated tracing paper in a standard laboratory desiccator to remove traces of organic solvent prior. We use a circular hole punch (AIEX, 3mm diameter), to punch out two 3 mm disks of lipid coated tracing paper. We punch the circular disk with the lipid coated side facing down ensuring that the lipid does not transfer to the punch. We use one 3 mm disk of lipid coated tracing paper per PCR tube for a total of two samples. We prechill the 0.5 mL PCR tube circular disk in a 4 °C incubator for 1 hour before placing the lipid coated paper face up into the tube. We allow the paper to incubate for a further 5 minutes in the 4 °C incubator. Working on ice, we mix 12 µL of the myTXTL mix as described in the myTXTL manual.[46] We place the mixture on top of the paper, close the tube, and incubate for 1 hour at 4 °C to prevent premature expression. While still working in the incubator, we harvest by pipetting 10 µL of the hydrating solution with a cut 100 µL pipet tip 6× on the coated

tracing paper to cover the whole area. We remove the tubes from the incubator and pool the two samples together in one 2 mL Eppendorf tube. We allow the tube to sit for 5 minutes to come to room temperature and add 80 µL of room temperature 2.8× PBS for a total volume of ~100 µL. This concentration of PBS was isomolar to the myTXTL mixture (~845 mOsm/kg) which ensured osmotic balance of the GUVs. We centrifuge the pooled samples for 60 minutes at 100×g in a swing bucket clinical centrifuge (AccuSpin 8c) equipped with 3D printed adapters for 2 mL Eppendorf tubes. We then remove 80 µL of the supernatant and resuspend the GUVs in the remaining solution by pipetting 6 times. We place the suspension in a 3 mm circular PDMS imaging chamber, place a coverslip, and incubate the reaction at room temperature (22 ºC) for 6 hours. For the negative control, we followed the same protocol but omitted the T7 deGFP control plasmid from the reaction mixture.

myTXTL expression imaging and image processing

We sediment the GUVs in a custom circular 3.5 mm diameter PDMS chamber. We obtain confocal images of the harvested GUVs using an upright confocal laser-scanning microscope (LSM 880, Axio Imager.Z2m, Zeiss, Germany) with a 20× Plan-Apochromat objective with a numerical aperture of 1.0. We capture images with an area of 212.55 µm × 212.55 µm, (1784 pixels × 1784 pixels). We measured the fluorescent intensity of the lumen of all the GUVs from 1 image per sample using FIJI. We draw circular ROIs wholly within the dark lumen of the GUVs and avoid selecting the bright pixels that correspond to the membrane. We ignore out of focus GUVs and bright objects which are non-GUVs. We follow the same procedure for the negative control except we use a 5.9 mm × 5.9 mm × 1 mm. We measured the intensity of GUVs in 5 images to get ~500 GUVs. We estimate the total number of GUVs in the chamber by dividing the number of GUVs in an image and multiplying with the total area of the chamber.

Actin encapsulation

We deposit 10 μg of DOPC:PEG2000-DSPE:PEG2000-Biotin-DSPE:Rhodamine-DOPE 95.9:3:1:0.1 mol %. on a 9.5 mm diameter disc of tracing paper. We place the lipid coated tracing paper in a standard laboratory desiccator to remove traces of organic solvent prior. We use a circular hole punch (AIEX, 3mm diameter), to punch out three 3 mm disks of lipid coated tracing paper. We punch the circular disk with the lipid coated side facing down ensuring that the lipid does not transfer to the punch. We use one 3 mm disk per PCR tube for a total of three samples. Working in a 4°C cold room for the duration of the experiment, we prechill the circular disk of lipid coated ULGT tracing paper and the 0.5 mL PCR tube for 5 minutes at 4 °C. We mix 12 μM actin mix (90:10 actin:ATTO-488 actin), 1 mM DTT, 300 mM sucrose and 1.8 μM fascin in 1× general actin buffer and 1× actin polymerization buffer on ice and immediately hydrate the lipid disks with 12 μL of the actin solution. We wrap the PCR tubes with aluminum foil and allow the samples to incubate for 1 hour at 4 °C. We harvest by pipetting 10 μL of the hydrating solution with a cut 100 μL pipet tip 6 times on the coated tracing paper to cover the whole area. We pool the three samples together in one 2 mL Eppendorf tube and add 200 μL of isomolar sedimentation buffer made of 1× general actin buffer, 1× actin polymerization buffer, 1 mM DTT and 300 mM glucose for a total volume of ~230 μL. We centrifuge the pooled samples for 20 minutes at 100×g in a swing bucket clinical centrifuge (AccuSpin 8c) equipped with 3D printed adapters for 2 mL Eppendorf tubes. We then remove 210 μL of the supernatant and resuspend the GUVs in the remaining solution by pipetting gently 6 times.

Actin imaging and image processing

GUVs imaged on the Nikon Ti2-E were bound to the coverslip through biotin-streptavidin linkers. GUVs imaged on the Zeiss LSM880 were imaged unbound. For bound GUVs, we prepare biotin functionalized coverslips as previously described.[17] We place 3.5 mm circular PDMS chambers on the functionalized coverslips and allow 10 μL of 0.1 mg/mL streptavidin to incubate in the chamber for 15 minutes. We then wash the chamber 6 times with 1× PBS, then 2 times with the sedimentation buffer. We add 20 μL of the GUV suspension into the chamber and allow the GUVs to sediment for 3 hours in a closed 150 mm Petri dish with a reservoir of water to prevent evaporation. We then remove unbound GUVs by removing 10 μL of the solution from the top of the sedimentation chamber, careful not to contact the surface of the coverslip. We then add 10 μL of sedimentation buffer and seal the chamber with a glass slide. We allow the samples to incubate in the same humidity chamber for a further 21 hours for a total of 24 hours before imaging. We note that actin bundles in the lumen of the GUVs are visible after the sedimentation process (~3 hours after harvesting). For unbound GUVs, we add 20 μL of the GUV suspension into a circular 3.5 mm diameter PDMS chamber. We allow the samples to incubate in the chamber for a total of 24 hours before imaging. We place the samples in a 150 mm Petri dish with a reservoir of water to prevent evaporation during the incubation process.

We image sample 1 using an upright confocal laser-scanning microscope (LSM 880, Axio Imager.Z2m, Zeiss, Germany) with a 20× Plan-Apochromat objective with a numerical aperture of 1.0. We image confocal Z-stacks from the bottom to the top of the GUV using a pinhole of 1 A.U. (592 pixels × 592 pixels, slice interval 0.667 μm).

We image sample 2 using an inverted microscope (Nikon Ti2-E with AxR point scanning confocal) equipped with an NSPARC detector, a CFI Plan Apo Lambda S 60XC Silicone Immersion Objective with a numerical aperture of 1.3 to capture confocal Z-stacks. We image

confocal Z-stacks from the bottom to the top of the GUVs using a pinhole of 2 A.U. The images were 2048 pixels × 2048 pixels with a slice interval 0.316 µm.

Image processing was performed using FIJI. GUVs > 6.5 µm that were counted. Actin appearing as one single unbranched actin bundle connected into a ring that appeared in the equatorial region of the GUVs was classified as a ring. Ring-like is when actin bundles have branches or not connecting, network-like bundles have multiple bundles of actin. GUVs were binned based on the diameter with GUVs edges of 0.5 µm below and 0.5 µm above the nearest whole number. We estimate the total number of GUVs in the chamber by dividing the number of GUVs in an image and multiplying with the total area of the chamber.

Author contributions

A.B.S. conceived and directed the study. A.C. performed experiments and analyzed the data. V.V. performed the scale up experiments. J.P. performed preliminary experiments. A.B.S and A.C. wrote the manuscript. All authors have given approval to the final version of the manuscript.

Data availability

The data supporting this article have been included in the manuscript.

Conflicts of interest

There are no conflicts to declare.

Acknowledgements

This work was funded by the National Science Foundation through NSF CAREER DMR-1848573. The data in this work was collected, in part, with a confocal microscope acquired through the National Science Foundation MRI Award Number DMR-1625733, and a scanning electron microscope acquired through NASA Grant NNX15AQ01A that are housed and managed by the Imaging and Microscopy Core at UC Merced. We would like to thank Brad Bartholomai Ph.D. and our local team from Nikon Instruments for their assistance in obtaining the superresolution images of actin in GUVs. The schematic in figure 4 was created in BioRender. Cooper, A. (2025) https://BioRender.com/g69f517.

References

(1) Pazzi, J.; Subramaniam, A. B. Dynamics of giant vesicle assembly from thin lipid films. *J Colloid Interface Sci* **2024**, *661*, 1033–1045.

(2) Cooper, A.; Subramaniam, A. B. Ultrahigh yields of giant vesicles obtained through mesophase evolution and breakup. *Soft Matter* **2024**, *20*, 9547–9561.

(3) Pazzi, J.; Subramaniam, A. B. Nanoscale Curvature Promotes High Yield Spontaneous Formation of Cell-Mimetic Giant Vesicles on Nanocellulose Paper. *ACS Appl Mater Interfaces* **2020**, *12*, 56549–56561.

(4) Zhang, X.; Li, C.; Liu, F.; Mu, W.; Ren, Y.; Yang, B.; Han, X. High-throughput production of functional prototissues capable of producing NO for vasodilation. *Nat Commun* **2022**, *13*.

(5) Wu, J.; Wei, Y.; Lan, J.; Hu, X.; Gao, F.; Zhang, X.; Gao, Z.; Liu, Q.; Sun, Z.; Chen, R.; et al. Screening of Protein-Based Ultrasmall Nanozymes for Building Cell-Mimicking Catalytic Vesicles. *Small* **2022**, *18*, 2202145.

(6) Witkowska, A.; Jablonski, L.; Jahn, R. A convenient protocol for generating giant unilamellar vesicles containing SNARE proteins using electroformation. *Scientific Reports 2018 8:1* **2018**, *8*, 1–8.

(7) Cao, R.; Kumar, D.; Dinsmore, A. D. Vesicle-Based Gel via Polyelectrolyte-Induced Adhesion: Structure, Rheology, and Response. *Langmuir* **2021**, *37*, 1714–1724.

(8) Stachowiak, J. C.; Hayden, C. C.; Sasaki, D. Y. Steric confinement of proteins on lipid membranes can drive curvature and tubulation. *Proc Natl Acad Sci U S A* **2010**, *107*, 7781–7786.

(9) Su, W. C.; Ho, J. C. S.; Gettel, D. L.; Rowland, A. T.; Keating, C. D.; Parikh, A. N. Kinetic control of shape deformations and membrane phase separation inside giant vesicles. *Nature Chemistry 2023 16:1* **2023**, *16*, 54–62.

(10) Tsai, F. C.; Koenderink, G. H. Shape control of lipid bilayer membranes by confined actin bundles. *Soft Matter* **2015**, *11*, 8834–8847.

(11) Tsai, F. C.; Stuhrmann, B.; Koenderink, G. H. Encapsulation of active cytoskeletal protein networks in cell-sized liposomes. *Langmuir* **2011**, *27*, 10061–10071.

(12) Blanken, D.; Van Nies, P.; Danelon, C. Quantitative imaging of gene-expressing liposomes reveals rare favorable phenotypes. *Phys Biol* **2019**, *16*.

(13) Litschel, T.; Schwille, P. Protein Reconstitution Inside Giant Unilamellar Vesicles. *Annu Rev Biophys* **2021**, *50*, 525–548.

(14) Bashirzadeh, Y.; Moghimianavval, H.; Liu, A. P. Encapsulated actomyosin patterns drive cell-like membrane shape changes. *iScience* **2022**, *25*, 104236.

(15) Gonzales, D. T.; Yandrapalli, N.; Robinson, T.; Zechner, C.; Tang, T. Y. D. Cell-Free Gene Expression Dynamics in Synthetic Cell Populations. *ACS Synth Biol* **2022**, *11*, 205–215.

(16) Nishimura, K.; Tsuru, S.; Suzuki, H.; Yomo, T. Stochasticity in gene expression in a cell-sized compartment. *ACS Synth Biol* **2015**, *4*, 566–576.

(17) Li, A. Z. T.; LiWang, A.; Subramaniam, A. B. Insights into a clock's fidelity through vesicular encapsulation. *bioRxiv* **2024**, 2024.10.13.617916.

(18) Horger, K. S.; Estes, D. J.; Capone, R.; Mayer, M. Films of agarose enable rapid formation of giant liposomes in solutions of physiologic ionic strength. *J Am Chem Soc* **2009**, *131*, 1810–1819.
(19) Weinberger, A.; Tsai, F. C.; Koenderink, G. H.; Schmidt, T. F.; Itri, R.; Meier, W.; Schmatko, T.; Schröder, A.; Marques, C. Gel-assisted formation of giant unilamellar vesicles. *Biophys J* **2013**, *105*, 154–164.
(20) Cooper, A.; Girish, V.; Subramaniam, A. B. Osmotic Pressure Enables High-Yield Assembly of Giant Vesicles in Solutions of Physiological Ionic Strengths. *Langmuir* **2023**, *39*, 5579–5590.
(21) Miller-Chou, B. A.; Koenig, J. L. A review of polymer dissolution. *Progress in Polymer Science (Oxford)*. August 2003, pp 1223–1270.
(22) Etale, A.; Onyianta, A. J.; Turner, S. R.; Eichhorn, S. J. Cellulose: A Review of Water Interactions, Applications in Composites, and Water Treatment. *Chemical Reviews*. American Chemical Society March 8, 2023, pp 2016–2048.
(23) Trache, D.; Tarchoun, A. F.; Derradji, M.; Hamidon, T. S.; Masruchin, N.; Brosse, N.; Hussin, M. H. Nanocellulose: From Fundamentals to Advanced Applications. *Front Chem* **2020**, *8*, 535734.
(24) Chen, G.; Levin, R.; Landau, S.; Kaduri, M.; Adir, O.; Ianovici, I.; Krinsky, N.; Doppelt-Flikshtain, O.; Shklover, J.; Shainsky-Roitman, J.; et al. Implanted synthetic cells trigger tissue angiogenesis through de novo production of recombinant growth factors. *Proc Natl Acad Sci U S A* **2022**, *119*, e2207525119.
(25) Marsh, D. *Handbook of Lipid Bilayers*, 2nd ed.; CRC Press, 2013.
(26) Weakly, H. M. J.; Wilson, K. J.; Goetz, G. J.; Pruitt, E. L.; Li, A.; Xu, L.; Keller, S. L. Several common methods of making vesicles (except an emulsion method) capture intended lipid ratios. *Biophys J* **2024**, *123*, 3452–3462.
(27) Mora, N. L.; Hansen, J. S.; Gao, Y.; Ronald, A. A.; Kieltyka, R.; Malmstadt, N.; Kros, A. Preparation of size tunable giant vesicles from cross-linked dextran(ethylene glycol) hydrogels. *Chemical Communications* **2014**, *50*, 1953–1955.
(28) Parigoris, E.; Dunkelmann, D. L.; Murphy, A.; Wili, N.; Kaech, A.; Dumrese, C.; Jimenez-Rojo, N.; Silvan, U. Facile generation of giant unilamellar vesicles using polyacrylamide gels. *Sci Rep* **2020**, *10*, 1–10.
(29) Wang, M.; Liu, Z.; Zhan, W. Janus Liposomes: Gel-Assisted Formation and Bioaffinity-Directed Clustering. *Langmuir* **2018**, *34*, 7509–7518.
(30) Irastorza-lorenzo, A.; Sánchez-porras, D.; Ortiz-arrabal, O.; Frutos, M. J. de; Esteban, E.; Fernández, J.; Janer, A.; Campos, A.; Campos, F.; Alaminos, M. Evaluation of Marine Agarose Biomaterials for Tissue Engineering Applications. *International Journal of Molecular Sciences 2021, Vol. 22, Page 1923* **2021**, *22*, 1923.
(31) Vázquez-González, M. L.; Calpena, A. C.; Domènech, Ò.; Montero, M. T.; Borrell, J. H. Enhanced topical delivery of hyaluronic acid encapsulated in liposomes: A surface-dependent phenomenon. *Colloids Surf B Biointerfaces* **2015**, *134*, 31–39.
(32) Vasvani, S.; Kulkarni, P.; Rawtani, D. Hyaluronic acid: A review on its biology, aspects of drug delivery, route of administrations and a special emphasis on its approved marketed products and recent clinical studies. *Int J Biol Macromol* **2020**, *151*, 1012–1029.

(33) Pacheco-Quito, E.-M.; Ruiz-Caro, R.; Veiga, M.-D. Carrageenan: Drug Delivery Systems and Other Biomedical Applications. *Mar Drugs* **2020**, *18*, 1–39.
(34) Yegappan, R.; Selvaprithiviraj, V.; Amirthalingam, S.; Jayakumar, R. Carrageenan based hydrogels for drug delivery, tissue engineering and wound healing. *Carbohydrate Polymers*. Elsevier Ltd October 15, 2018, pp 385–400.
(35) Kim, C.; Jeong, D.; Kim, S.; Kim, Y.; Jung, S. Cyclodextrin functionalized agarose gel with low gelling temperature for controlled drug delivery systems. *Carbohydr Polym* **2019**, *222*, 115011.
(36) Lim, Y. M.; Gwon, H. J.; Choi, J. H.; Shin, J.; Nho, Y. C.; Jeong, S. I.; Chong, M. S.; Lee, Y. M.; Kwon, I. K.; Kim, S. E. Preparation and biocompatibility study of gelatin/kappa-carrageenan scaffolds. *Macromol Res* **2010**, *18*, 29–34.
(37) Stone, B. A.; Svensson, B.; Collins, M. E.; Rastall, R. A. Polysaccharide Degradation. *Glycoscience* **2008**, 2325–2375.
(38) Buhren, B. A.; Schrumpf, H.; Hoff, N. P.; Bölke, E.; Hilton, S.; Gerber, P. A. Hyaluronidase: from clinical applications to molecular and cellular mechanisms. *Eur J Med Res* **2016**, *21*, 5.
(39) Fraser, J. R. E.; Laurent, T. C.; Engström-Laurent, A.; Laurent, U. G. B. Elimination of hyaluronic acid from the blood stream in the human. *Clin Exp Pharmacol Physiol* **1984**, *11*, 17–25.
(40) Wang, K.; Liu, M.; Mo, R. Polysaccharide-Based Biomaterials for Protein Delivery. *Med Drug Discov* **2020**, *7*, 100031.
(41) Barrett, T.; Kobayashi, H.; Brechbiel, M.; Choyke, P. L. Macromolecular MRI contrast agents for imaging tumor angiogenesis. *Eur J Radiol* **2006**, *60*, 353–366.
(42) Sun, G.; Mao, J. J. Engineering Dextran-Based Scaffolds for Drug Delivery and Tissue Repair. *Nanomedicine* **2012**, *7*, 1771–1784.
(43) Lévesque, S. G.; Lim, R. M.; Shoichet, M. S. Macroporous interconnected dextran scaffolds of controlled porosity for tissue-engineering applications. *Biomaterials* **2005**, *26*, 7436–7446.
(44) Mazia, D.; Schatten, G.; Sale, W. Adhesion of cells to surfaces coated with polylysine. Applications to electron microscopy. *Journal of Cell Biology* **1975**, *66*, 198–200.
(45) Litschel, T.; Kelley, C. F.; Holz, D.; Adeli Koudehi, M.; Vogel, S. K.; Burbaum, L.; Mizuno, N.; Vavylonis, D.; Schwille, P. Reconstitution of contractile actomyosin rings in vesicles. *Nat Commun* **2021**, *12*.
(46) Daciel Arbor Biosciences. *myTXTL ® Pro Cell-Free Expression Kit Cell-Free Protein Expression System User Manual*; 2024.

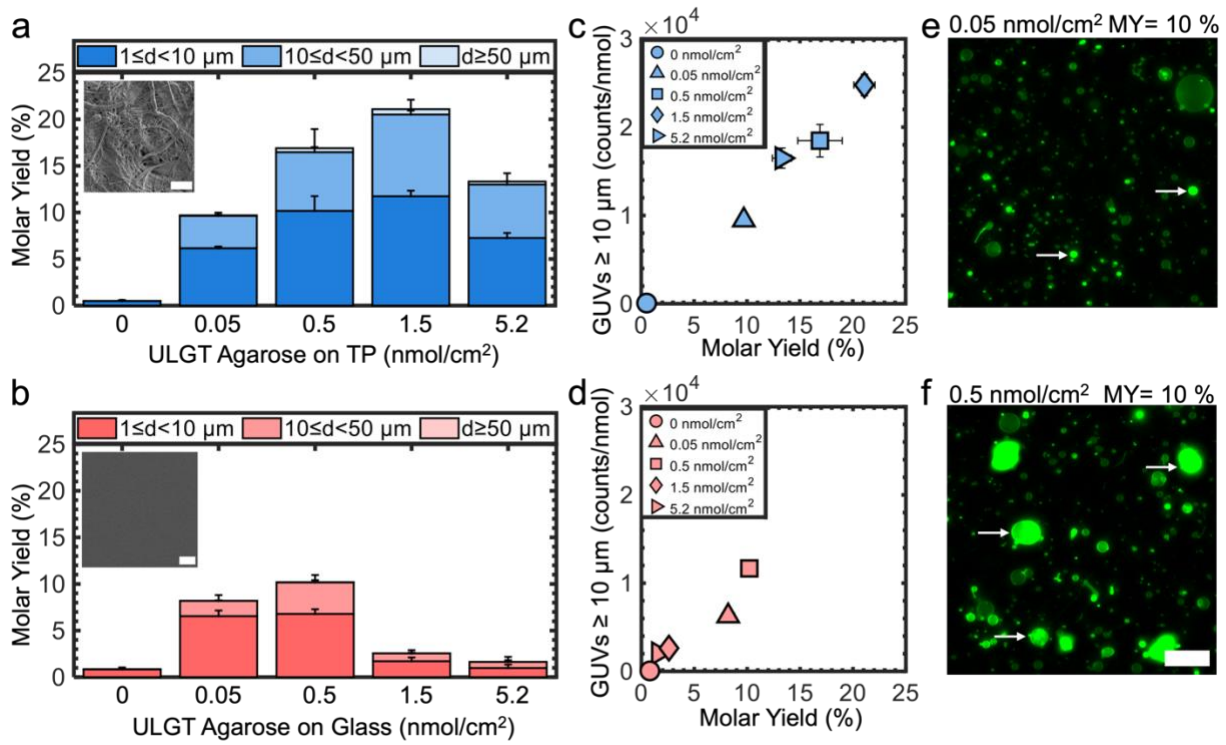

Figure 1. GUV yields from DOPC GUVs on ULGT agarose coated substrates. a) Stacked bar plots of GUV yields from ULGT agarose coated tracing paper. The inset shows a SEM image of nanocellulose tracing paper. b) Stacked bar plots of GUV yields from ULGT agarose coated glass slides. The inset shows a SEM image of glass. Each bar is split into 3 sections depending on the GUV diameter is the average of N=3 independent repeats. The error bars are one standard deviation from the mean. The scale bars on the insets are 2 µm. c) Scatter plot of GUVs ≥ 10 µm versus the molar yield from ULGT agarose coated tracing paper. d) Scatter plot of GUVs ≥ 10 µm versus the molar yield from ULGT agarose coated glass slides. Representative harvested objects from DOPC GUVs from ULGT coated substrates with the same molar yield, 10 %. e) 1.5 nmol/cm^2 ULGT agarose on tracing paper. f) 0.5 nmol/cm^2 ULGT agarose on glass slides. The white arrows point to examples of non-GUV structures. Scale bar is 50 µm.

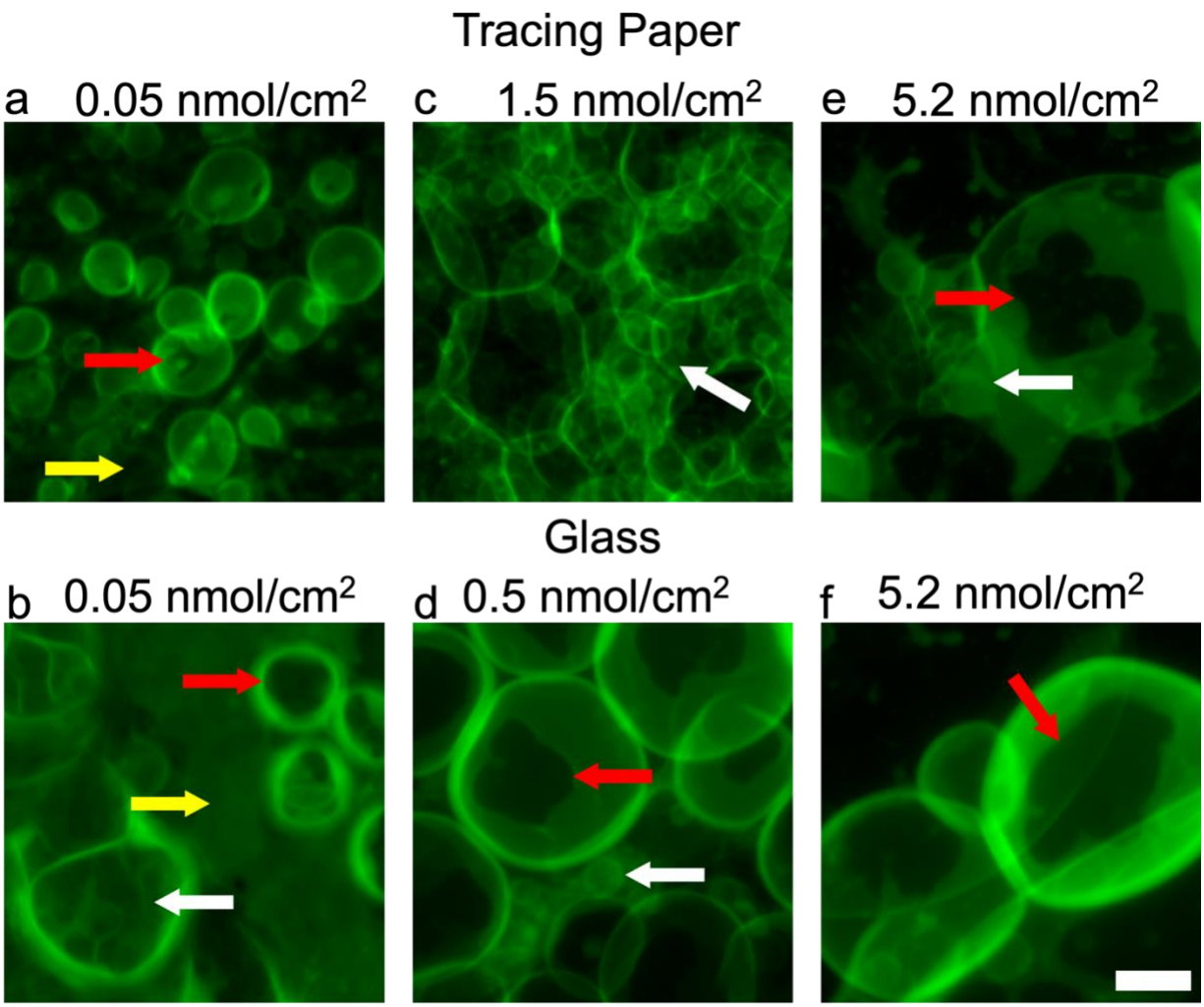

Figure 2. Surface morphology of DOPC on ULGT agarose coated substrates. The images are sum projections of Z-stacks from 100 µm from the surface. a) 0.05 nmol/cm^2 on tracing paper, b) 0.05 nmol/cm^2 on glass slides, c) 1.5 nmol/cm^2 on tracing paper, d) 0.05 nmol/cm^2 on glass slides, e) 5.2 nmol/cm^2 on tracing paper, and f) 5.2 nmol/cm^2 on glass slides. The red arrows point to delamination patterns in the buds. The white arrows point to fully formed GUV buds. The yellow arrows point to bilayer stacks that have not formed buds. Scale bar is 10 µm.

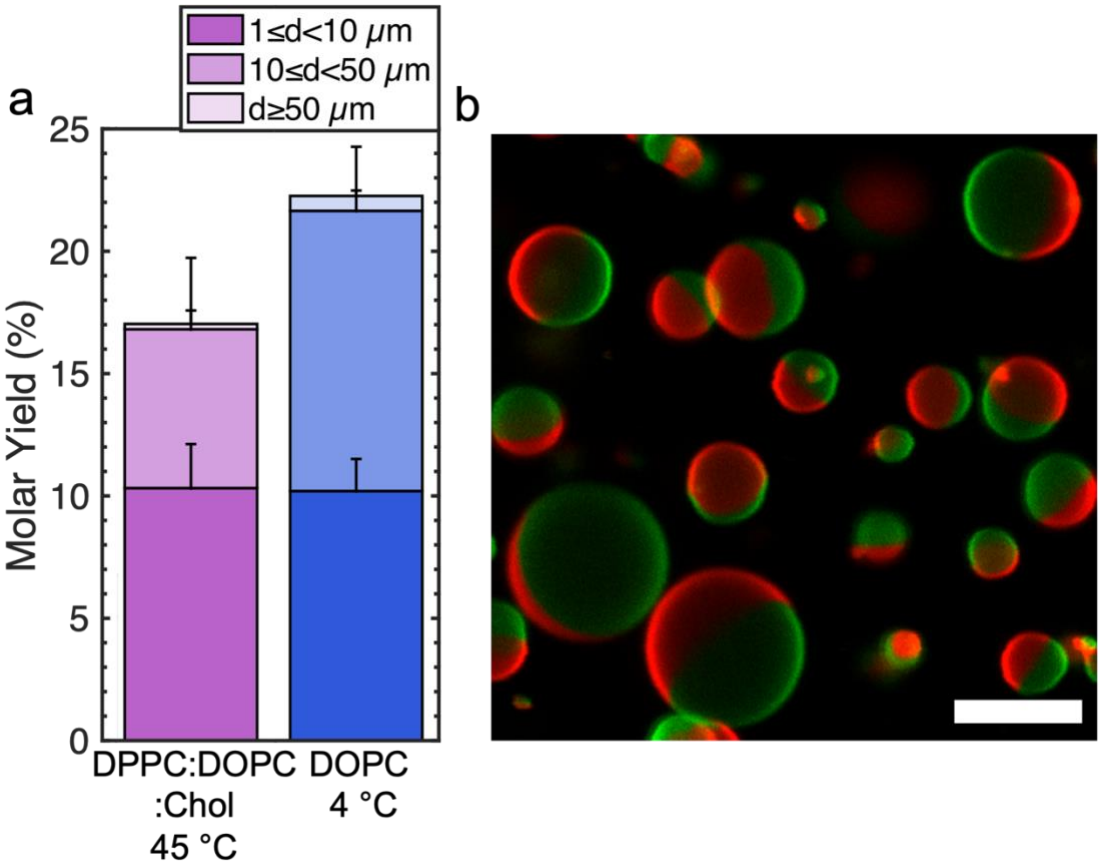

Figure 3. Molar yields of GUVs assembled at different temperatures a) Molar yield of phase separating GUVs assembled at 45 °C and DOPC GUVs assembled at 4°C from ULGT agarose coated tracing paper. All ULGT coated tracing paper was fabricated with a surface concentration of 1.5 nmol/cm^2. Each bar is split into 3 sections depending on the GUV diameter is the average of N=3 independent repeats. The error bars are one standard deviation from the mean. b) Representative image of phase separated vesicles assembled using DPPC:DOPC:Chol with 3 mol % PEG2000-DSPE at 45 °C. Scale bar is 50 µm.

Table 1 Molar yields and percent non-GUV objects from assembly on polymer-coated nanocellulose substrates. Each value is a mean ± standard deviation of N=3 independent repeats.

Polymer	Surface Concentration ($nmol/cm^2$)	Lipid Composition	Molar Yield (%)	GUV Counts ($\times 10^5$ GUVs/μg)	Percent non-GUVs (%)
4°C					
Dextran, 100 kDa	1.9	DOPC	18 ± 0.7	8.5 ± 0.8	10.1 ± 0.4
Hyaluronic Acid, 8-15 kDa	12.4	DOPC	20 ± 0.8	11 ± 0.6	8.1 ± 0.2
Hyaluronic Acid, 70-120 kDa	1.5	DOPC	13 ± 2.7	5.2 ± 1.6	9.8 ± 1.3
22 °C					
Poly-D-Lysine	2.9	DOPC	19 ± 3.0	6.8 ± 1.4	9.3 ± 1.9
Dextran, 100 kDa	4.3	DOPC	15 ± 0.3	5.8 ± 0.1	11 ± 0.1
Hyaluronic Acid, 8-15 kDa	12.4	DOPC	22 ± 2.5	10 ± 0.7	11 ± 0.1
Hyaluronic Acid, 70-120 kDa	1.5	DOPC	15 ± 2.0	5.2 ± 1.6	9.8 ± 1.3
Carrageenan	1.2	DOPC	16 ± 2.0	6.3 ± 1.2	7.0 ± 2.0
DNA, Single stranded from salmon testes	2.3	DOPC	6.7 ± 1.2	6.1 ± 1.4	9.7 ± 0.3
Bovine Serum Albumin	2.8	DOPC	6.1 ± 0.5	3.4 ± 0.4	11 ± 0.7
45°C					
Hyaluronic Acid, 8-15 kDa	12.4	DOPC:DPPC: Chol	18 ± 2.2	8.4 ± 1.6	16 ± 1.1

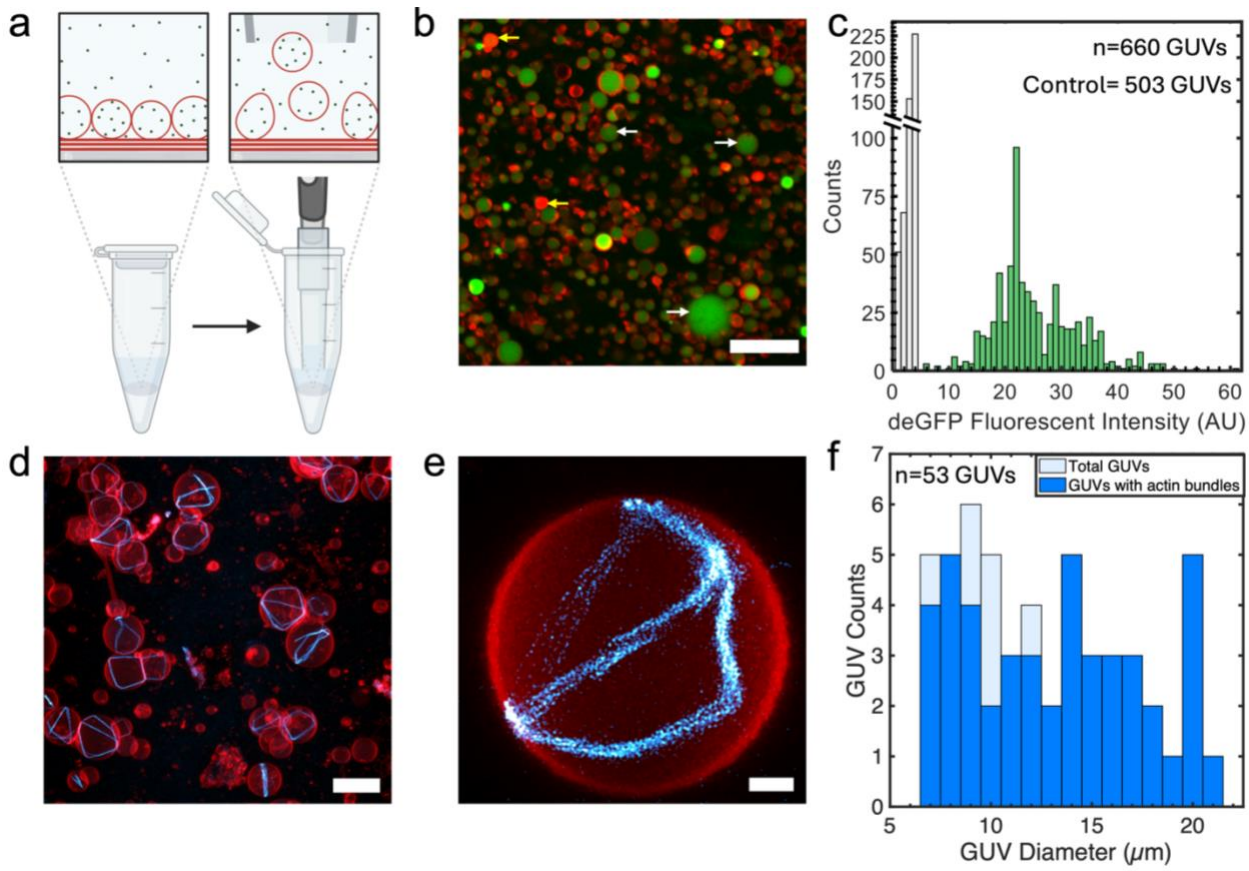

Figure 4. Encapsulation using ULGT agarose coated tracing paper. a) Schematic of small scale encapsulation of myTXTL cell free expression kit. b) Representative harvested image of GUVs with encapsulation of myTXTL cell free expression kit. White arrows point to examples of GUVs. Yellow arrows point to examples of non-GUVs that are not counted. Scale bar is 20 µm. c) Histogram of fluorescent intensities from encapsulation of myTXTL cell free expression kit with deGFP control plasmid. N=1, 660 GUVs counted. The grey shows the distribution of intensity of the control that lacked the plasmid. Note the average intensities in the lumen were below 5 A.U. Encapsulation of actin bundles forming ring-like structures. d) Representative image of GUVs with actin bundles. Scale bar is 20 µm. e) Single GUV with encapsulation of an actin bundle. Scale bar is 2 µm. f) Fraction of actin bundles seen in GUVs vs the diameter of GUVs. n = 53 GUVs counted.

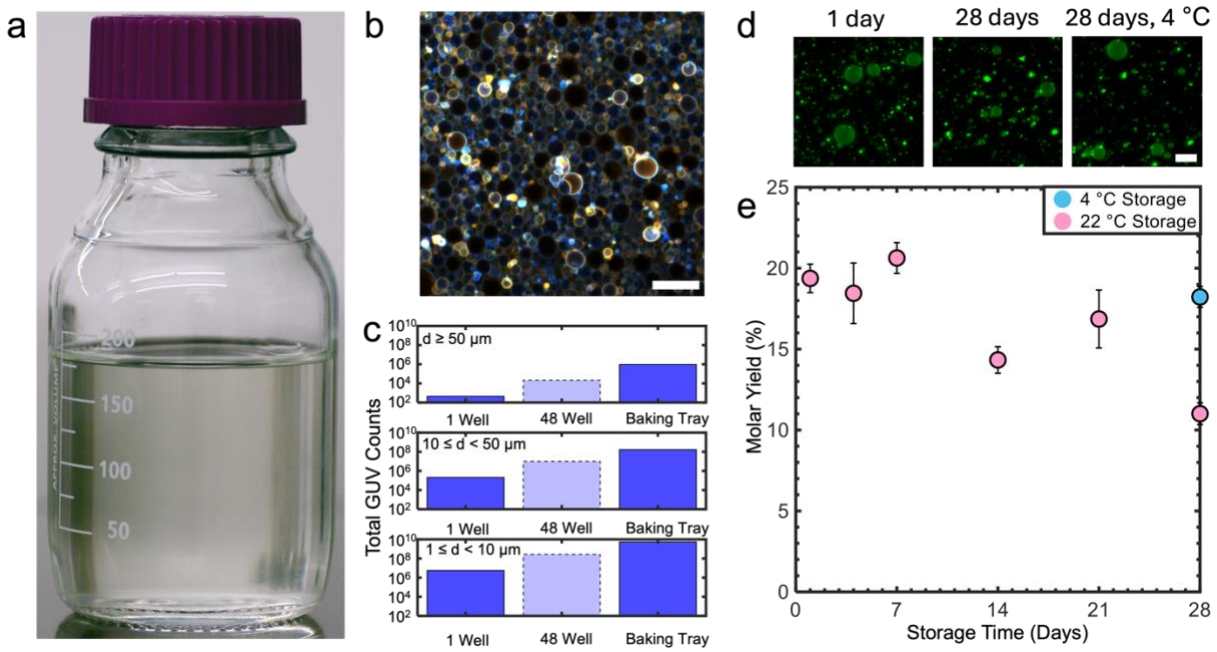

Figure 5. Large scale assembly of GUVs using dextran coated tracing paper and ULGT agarose coated tracing paper storage. a) Photograph of 188 mL of a suspension of GUVs obtained by hydrating a 11-in × 7-in sheet of paper in a baking tray. The concentration of GUVs was 2.95 × 10^7 per mL for a total of 5.54 × 10^9 GUVs b) Representative images of concentrated GUV pellet obtained after centrifugation. c) Bar plots of total GUV counts from 1 well, 48 wells calculated from the counts of assembly in 1 well, and the large-scale baking tray. The bar plots are split into 3 sections based on GUV diameter, d, $1 \leq d < 10$ µm, $10 \leq d < 50$ µm and $d \geq 50$ µm. Note the logarithmic scale on the y-axis. Single well data repeated from Table 1. d) Representative images of assembly from ULGT tracing paper stored for 1 day at 22 °C, 28 days at 22 °C and 28 days at 4 °C. Scale bar is 50 µm. e) Molar yield of GUV assembly over time using stored tracing paper.